

Formulating Compressive Strength of Dust Aggregates from Low to High Volume Filling Factors with Numerical Simulations

MISAKO TATSUUMA ^{1,2}, AKIMASA KATAOKA ², SATOSHI OKUZUMI ¹ AND HIDEKAZU TANAKA ³

¹*Department of Earth and Planetary Sciences, Tokyo Institute of Technology, 2-12-1 Ookayama, Meguro-ku, Tokyo 152-8551, Japan*

²*Division of Science, National Astronomical Observatory of Japan, 2-21-1 Osawa, Mitaka, Tokyo 181-8588, Japan*

³*Astronomical Institute, Tohoku University, 6-3 Aramaki, Aoba-ku, Sendai, Miyagi 980-8578, Japan*

(Received December 7, 2022; Revised April 27, 2023; Accepted June 15, 2023)

Submitted to ApJ

ABSTRACT

Compressive strength is a key to understanding the internal structure of dust aggregates in protoplanetary disks and their resultant bodies, such as comets and asteroids in the Solar System. Previous work has modeled the compressive strength of highly-porous dust aggregates with volume filling factors lower than 0.1. However, a comprehensive understanding of the compressive strength from low (< 0.1) to high (> 0.1) volume filling factors is lacking. In this paper, we investigate the compressive strength of dust aggregates by using aggregate compression simulations resolving constituent grains based on JKR theory to formulate the compressive strength comprehensively. We perform a series of numerical simulations with moving periodic boundaries mimicking the compression behavior. As a result, we find that the compressive strength becomes sharply harder when the volume filling factor exceeds 0.1. We succeed in formulating the compressive strength comprehensively by taking into account the rolling motion of aggregates for low volume filling factors and the closest packing of aggregates for high volume filling factors. We also find that the dominant compression mechanisms for high volume filling factors are sliding and twisting motions, while rolling motion dominates for low volume filling factors. We confirm that our results are in good agreement with previous numerical studies. We suggest that our analytical formula is consistent with the previous experimental results if we assume the surface energy of silicate is $\simeq 210 \pm 90$ mJ m⁻². Now, we can apply our results to properties of small compact bodies, such as comets, asteroids, and pebbles.

Keywords: Planet formation (1241) — Protoplanetary disks (1300) — Planetesimals (1259) — Astronomical simulations (1857) — Analytical mathematics (38) — Computational astronomy (293)

1. INTRODUCTION

The first step of planet formation is the coagulation of (sub)micron-sized dust grains. The aggregations of dust grains are called dust aggregates (e.g., Smirnov 1990; Meakin 1991; Ossenkopf 1993; Dominik & Tielens 1997; Wurm & Blum 1998; Kempf et al. 1999; Blum & Wurm 2000; Krause & Blum 2004; Paszun & Dominik 2006, 2008, 2009; Wada et al. 2007, 2008, 2009, 2013; Suyama

et al. 2008, 2012; Okuzumi et al. 2009; Geretshauser et al. 2010, 2011). In the first stage of dust growth, a dust aggregate hits another aggregate and sticks to it. This process produces fractal aggregates called ballistic cluster-cluster aggregates (BCCAs, e.g., Mukai et al. 1992). The coagulation of dust aggregates leads to the formation of planetesimals, which are kilometer-sized building blocks of planets (e.g., Okuzumi et al. 2012; Kataoka et al. 2013a). There is another scenario that dust aggregates grow into millimeter-sized compact pebbles, and pebbles coagulate to form planetesimals by some instabilities or collisions (e.g., Johansen et al. 2007; Windmark et al. 2012; Davidsson et al. 2016; Wahlberg

Jansson et al. 2017; Yang et al. 2017; Lorek et al. 2018; Fulle et al. 2019). In this scenario, planetesimals are pebble aggregates whose internal structure is different from dust aggregates in this work.

Compression of dust aggregates is a key process during their growth. There are several compression mechanisms: collisional, disk gas, and self-gravity compression. Some numerical studies have shown that collisional compression is not sufficient and aggregates' internal densities remain $\sim 10^{-5} \text{ g cm}^{-3}$ (e.g., Okuzumi et al. 2012; Kataoka et al. 2013a). Some experimental studies suggest that the bouncing of dust aggregates leads to compaction (e.g., Krijt et al. 2018), but numerical simulation studies suggest that the bouncing of highly porous dust aggregates hardly occurs (e.g., Wada et al. 2011). As for disk gas and self-gravity compression, the compressive strength of dust aggregates determines their internal densities (e.g., Blum & Schr ppler 2004; Paszun & Dominik 2008; G ttler et al. 2009; Seizinger et al. 2012; Kataoka et al. 2013b,a; Omura & Nakamura 2017). The compressive strength also determines the internal structures of larger bodies, such as planetesimals, asteroids, and comets (e.g., Omura & Nakamura 2018, 2021).

Kataoka et al. (2013b) have modeled the compressive strength of highly-porous dust aggregates with volume filling factors lower than 0.1. They have analytically formulated the compressive strength by using the volume filling factor and several material parameters, such as monomer (constituent grain) radius and surface energy.

However, a comprehensive understanding of the compressive strength from low (< 0.1) to high (> 0.1) volume filling factors is lacking. The compressive strength for high volume filling factors is necessary for applications to comets, asteroids, and pebbles, while for low volume filling factors is necessary for dust growth. Some studies investigated the compressive strength for volume filling factors above 0.1 (e.g., Blum & Schr ppler 2004; Paszun & Dominik 2008; G ttler et al. 2009; Seizinger et al. 2012; Omura & Nakamura 2017, 2018). However, the dependences on material parameters are still unclear and there is a discrepancy between low and high volume filling factors.

In this work, we perform numerical simulations of the compression of dust aggregates and formulate the compressive strength that can treat a full range of volume filling factors. We use the same simulation code as Kataoka et al. (2013b), but we calculate the compressive strength to high volume filling factors to apply it to small bodies in the Solar System with volume filling factors higher than 0.1. We also investigate the dependences on material parameters, such as monomer radius and surface energy. Finally, we construct a corrected

analytical formula of the compressive strength of dust aggregates based on a simple model to apply it to other parameters.

This paper is organized as follows. In Section 2, we explain our simulation settings and a monomer interaction model based on Dominik & Tielens (1997) and Wada et al. (2007). Our simulation settings, such as initial conditions, boundary conditions, and calculation of compressive strength, are the same as those of Kataoka et al. (2013b). In Section 3, we show our results of numerical simulations to derive the compressive strength of dust aggregates. We show fiducial runs, and then we investigate the parameter dependences. In Section 4, we discuss parameter dependences and the physics behind the compression of dust aggregates. We show a corrected analytical formula of compressive strength and energy dissipation mechanisms during the compression. Then, we compare our results with previous experimental and numerical studies to confirm the validity of our results and discuss interpretations of previous results. Finally, we conclude our work in Section 5.

2. SIMULATION SETTINGS

In this section, we explain our simulation settings. First, we introduce a monomer interaction model based on Dominik & Tielens (1997) and Wada et al. (2007) in Section 2.1. We also explain an artificial normal damping force. Second, we describe the outline of our simulations, where we use periodic boundaries and move them to calculate the compressive strength in Section 2.2. We also explain the initial conditions and the velocity at the computational boundaries. Third, we explain the method to calculate the compressive strength and volume filling factor in Section 2.3.

2.1. Monomer Interaction Model

We calculate the interactions of spherical monomers in contact by using a theoretical model of Dominik & Tielens (1997) and Wada et al. (2007) based on JKR theory (Johnson et al. 1971). There are four kinds of interactions in this model: normal direction, sliding, rolling, and twisting motions. The material parameters that are needed to describe the model are the monomer radius r_0 , material density ρ_0 , surface energy γ , Poisson's ratio ν , Young's modulus E , and the critical rolling displacement ξ_{crit} . We list the material parameters of ice and silicate in Table 1. We set the same values to compare our results with those of Kataoka et al. (2013b).

We explain the rolling behavior of two monomers in contact as a consequence of rolling motion dominating during the compression of dust aggregates with volume filling factors lower than 0.1 (Kataoka et al. 2013b). Two

monomers roll irreversibly after the absolute value of the rolling displacement exceeds the critical limit ξ_{crit} . The critical rolling displacement has different values between the theoretical one ($\xi_{\text{crit}} = 2 \text{ \AA}$, Dominik & Tielens 1997) and the experimental one ($\xi_{\text{crit}} = 32 \text{ \AA}$, Heim et al. 1999). We adopt $\xi_{\text{crit}} = 8 \text{ \AA}$ as a fiducial value of ice according to Kataoka et al. (2013b) and investigate the dependence of our results on ξ_{crit} in Section 3.2. The energy needed for a monomer to roll a distance of $(\pi/2)r_0$ is given as

$$\begin{aligned} E_{\text{roll}} &= 6\pi^2 \gamma r_0 \xi_{\text{crit}} \\ &\simeq 4.7 \times 10^{-16} \text{ J} \\ &\times \left(\frac{\gamma}{100 \text{ mJ m}^{-2}} \right) \left(\frac{r_0}{0.1 \text{ \mu m}} \right) \left(\frac{\xi_{\text{crit}}}{8 \text{ \AA}} \right). \end{aligned} \quad (1)$$

For details, see Sections 2.2.2 and 3 of Wada et al. (2007).

We add an artificial normal damping force proportional to a dimensionless damping coefficient k_n . For details, see Section 2.2 of Tatsuuma et al. (2019). The force in the normal direction induces oscillations of two monomers in contact. In reality, the oscillations would decay because of viscoelasticity or hysteresis of monomers (e.g., Greenwood & Johnson 2006; Tanaka et al. 2012; Krijt et al. 2013). We adopt $k_n = 0.01$ according to Kataoka et al. (2013b), although they have revealed that the damping coefficient does not change the compressive strength.

2.2. Compression Simulation Setups

The outline of our numerical simulations is as follows (see also Figure 1). First, we randomly create a BCCA. Second, we compress it sufficiently slowly and isotropically by moving periodic boundaries. For details of the periodic boundary conditions, see Section 2.3 of Kataoka et al. (2013b).

The velocity at the computational boundaries is given as

$$v_b = -\frac{C_v}{t_c} L, \quad (2)$$

where C_v is a constant dimensionless strain-rate parameter, t_c is the characteristic time (Wada et al. 2007), and L is the length of the computational box. The characteristic time is given as

$$\begin{aligned} t_c &= 0.95 \frac{r_0^{7/6} \rho_0^{1/2}}{\gamma^{1/6} E^{*1/3}} \\ &\simeq 1.9 \times 10^{-10} \text{ s} \left(\frac{\gamma}{100 \text{ mJ m}^{-2}} \right)^{-1/6} \left(\frac{r_0}{0.1 \text{ \mu m}} \right)^{7/6} \\ &\times \left(\frac{\rho_0}{1 \text{ g cm}^{-3}} \right)^{1/2} \left(\frac{E^*}{3.73 \text{ GPa}} \right)^{-1/3}, \end{aligned} \quad (3)$$

where E^* is the reduced Young's modulus of Young's moduli E_1 and E_2 defined as

$$\frac{1}{E^*} = \frac{1 - \nu_1^2}{E_1} + \frac{1 - \nu_2^2}{E_2}. \quad (4)$$

Here, we assume $E_1 = E_2 = E$ and $\nu_1 = \nu_2 = \nu$, and therefore $E^* = E/[2(1 - \nu^2)]$. We can also describe the absolute value of the velocity at the computational boundaries as

$$\begin{aligned} |v_b| &\simeq 0.21 \text{ cm s}^{-1} \left(\frac{\gamma}{100 \text{ mJ m}^{-2}} \right)^{1/6} \left(\frac{r_0}{0.1 \text{ \mu m}} \right)^{-1/6} \\ &\times \left(\frac{\rho_0}{1 \text{ g cm}^{-3}} \right)^{-1/2} \left(\frac{E^*}{3.73 \text{ GPa}} \right)^{1/3} \left(\frac{C_v}{1 \times 10^{-7}} \right) \\ &\times \left(\frac{N}{16384} \right)^{1/3} \phi^{-1/3}, \end{aligned} \quad (5)$$

where N is the number of monomers and ϕ is the volume filling factor.

We adopt $C_v = 1 \times 10^{-7}$ as a fiducial value because the larger C_v , the higher pressure we need for the compression of low-density dust aggregates (Kataoka et al. 2013b). For other parameter sets, we adopt $C_v = 3 \times 10^{-7}$ because simulations of low C_v are time-consuming.

2.3. Compressive Strength and Volume Filling Factor Measurements

We calculate the compressive strength P_{calc} in the way described in Section 2.4 of Kataoka et al. (2013b). We calculate the translational kinetic energy per unit volume and the sum of the forces acting at all connections per unit volume as

$$P_{\text{calc}} = \frac{2K}{3V} + \frac{1}{3V} \left\langle \sum_{i < j} (\mathbf{x}_i - \mathbf{x}_j) \cdot \mathbf{f}_{i,j} \right\rangle_t, \quad (6)$$

where V is the volume of the computational box, K is the time-averaged kinematic energy of all monomers given as

$$K = \left\langle \sum_{i=1}^N \frac{m_0}{2} \left(\frac{d\mathbf{x}_i}{dt} \right)^2 \right\rangle_t, \quad (7)$$

m_0 is the monomer mass, \mathbf{x}_i is the coordinates of monomer i , $\langle \rangle_t$ is a long-time average, and $\mathbf{f}_{i,j}$ is the force from monomer j on monomer i . For details of the derivation of compressive strength, see Appendix A. In our simulations, the second term on the right-hand side of Equation (6) dominates the compressive strength.

We also calculate the volume filling factor of dust aggregates as

$$\phi_{\text{calc}} = \frac{(4/3)\pi r_0^3 N}{V}. \quad (8)$$

Table 1. Material parameters of ice and silicate

Parameter	Ice 0.1 μm (fiducial)	Ice (others)	Ice 1.0 μm	Silicate 0.1 μm	Silicate 1.0 μm
Monomer radius r_0 (μm)	0.1	0.1	1.0	0.1	1.0
Material density ρ_0 (g cm^{-3})	1.0	1.0	1.0	2.65	2.65
Surface energy γ (mJ m^{-2})	100	100	100	20	20
Poisson's ratio ν	0.25	0.25	0.25	0.17	0.17
Young's modulus E (GPa)	7	7	7	54	54
Critical rolling displacement ξ_{crit} (\AA)	8	2, 4, 16, 32	8	20	20
The number of monomers N	16384	16384	16384	16384	16384
Strain rate parameter C_v	1×10^{-7}	3×10^{-7}	1×10^{-7}	1×10^{-7}	1×10^{-7}
Damping coefficient k_n	0.01	0.01	0.01	0.01	0.01

NOTE—We use ρ_0 , γ , ν , E , and ξ_{crit} of ice of [Israelachvili \(1992\)](#) and [Dominik & Tielens \(1997\)](#) and of silicate of [Seizinger et al. \(2012\)](#).

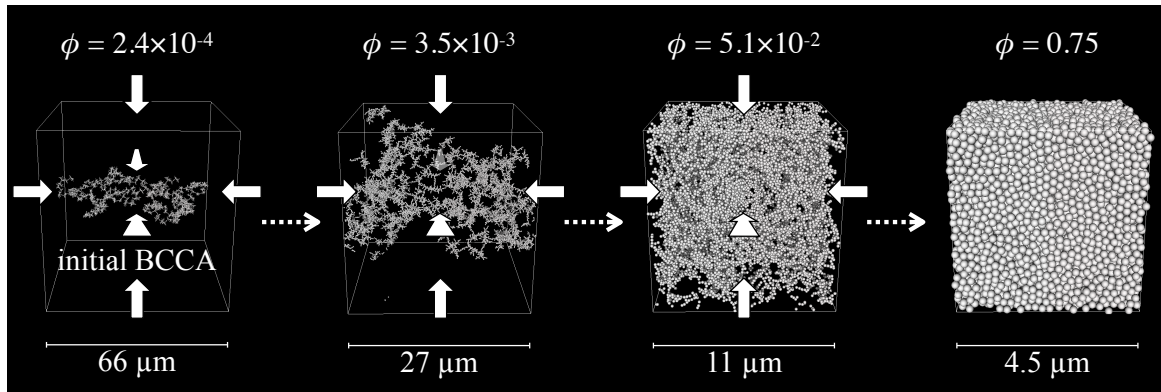


Figure 1. Outline of our simulations. Each aggregate contains 16384 ice monomers with a radius of 0.1 μm . Each white cube shows the computational box with periodic boundaries. We compress it three-dimensionally as shown by the white allows. We put each volume filling factor and size of the computational box above and below each snapshot, respectively. In our simulations, the final volume filling factor can exceed a value for the closest packing $\sqrt{2}\pi/6 = 0.74$ because monomers can deform elastically.

We take an average of the compressive strength P_{calc} (Equation (6)) and the volume filling factor ϕ_{calc} (Equation (8)) for every 10,000 time-steps. One time-step in our simulations is $0.1t_c = 1.9 \times 10^{-11}$ s and 10,000 time-steps correspond to 1.9×10^{-7} s.

3. NUMERICAL RESULTS

In this section, we report the results of numerical simulations to derive the compressive strength of dust aggregates. We perform 10 simulations with different BC-CAs and take an average of them for every parameter set to reduce the effect of different monomer configurations. First, we show the results of fiducial runs in Section 3.1. Then, we investigate the parameter dependences in Section 3.2. [Kataoka et al. \(2013b\)](#) confirmed that the results do not depend on any numerical parameters: the number of monomers N , the strain rate

parameter C_v , and the damping coefficient k_n . For the dependence on the numerical parameters, see Appendix B.

3.1. Fiducial Runs

Figure 2 shows the compressive strength of 10 runs and an average of them for the fiducial parameter set. The dotted line shows the analytical formula of [Kataoka et al. \(2013b\)](#),

$$\begin{aligned}
 P_{\text{K13}} &= \frac{E_{\text{roll}}}{r_0^3} \phi^3 \\
 &\simeq 4.7 \times 10^5 \text{ Pa} \\
 &\quad \times \left(\frac{\gamma}{100 \text{ mJ m}^{-2}} \right) \left(\frac{r_0}{0.1 \mu\text{m}} \right)^{-2} \left(\frac{\xi_{\text{crit}}}{8 \text{ \AA}} \right) \phi^3 \quad (9)
 \end{aligned}$$

Our averaged simulation result is consistent with Equation (9) when $\phi \lesssim 0.1$. However, we find that the mea-

sured compressive strength for $\phi > 0.1$ is significantly higher than predicted from Equation (9). We note that the compressive strength measured in each run has a large scatter.

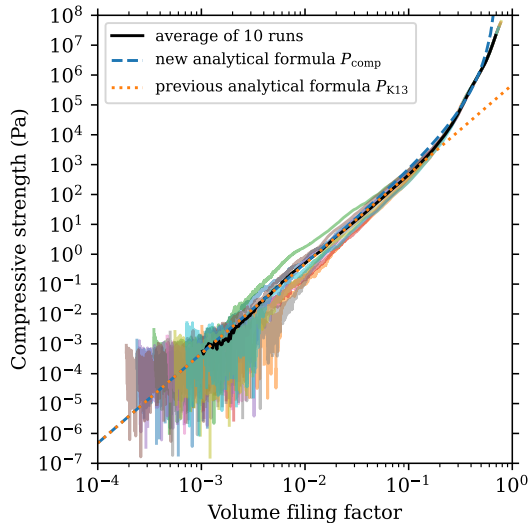


Figure 2. Compressive strength against volume filling factor of dust aggregates that contain ice monomers of $0.1\text{-}\mu\text{m}$ radius. The colored solid lines show the results for 10 different initial BCCAs. The black solid line shows the average of the 10 runs. The dashed line shows our corrected analytical formula (Equation (11)). The dotted line shows the analytical formula (Equation (9)) of Kataoka et al. (2013b).

3.2. Parameter Dependences

We find that the compressive strength does not depend on the critical rolling displacement ξ_{crit} when $\phi \gtrsim 0.3$. This is shown in Figure 3, where we plot compressive strength when $\xi_{\text{crit}} = 2, 4, 8, 16,$ and 32 \AA . In contrast, when $\phi \lesssim 0.3$, the compressive strength has a dependence on ξ_{crit} because the dominant mechanism of energy dissipation is rolling motion. An exception is when $\xi_{\text{crit}} = 32 \text{ \AA}$, for which the compressive strength curve is nearly identical to that for $\xi_{\text{crit}} = 16 \text{ \AA}$. This is because the dominant mechanism of energy dissipation for $\xi_{\text{crit}} > 16 \text{ \AA}$ is twisting motion (Kataoka et al. 2013b). We note that the difference in compressive strength due to ξ_{crit} is about the same as the difference per run.

As for the dependences on the other material parameters, we find that the scaling predicted from Equation (9) that the compressive strength scales as $P \propto \gamma \xi_{\text{crit}} r_0^{-2}$ no longer applies for $\phi > 0.1$. This is shown in Figure 4, where we plot the compressive strength in the four cases (ice $0.1 \mu\text{m}$, ice $1.0 \mu\text{m}$, silicate $0.1 \mu\text{m}$, and silicate $1.0 \mu\text{m}$) listed in Table 1. The dotted lines show

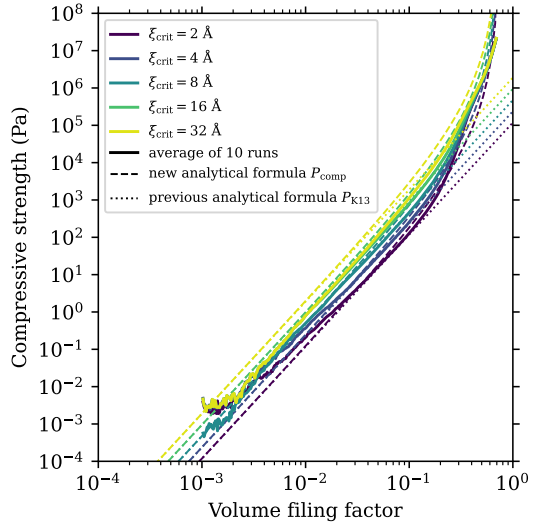


Figure 3. Compressive strength against volume filling factor of dust aggregates that contain ice monomers of $0.1\text{-}\mu\text{m}$ radius with different critical rolling displacements ξ_{crit} . The critical rolling displacements are $\xi_{\text{crit}} = 2, 4, 8, 16,$ and 32 \AA from dark to light colors. We adopt $C_v = 3 \times 10^{-7}$ for $\xi_{\text{crit}} = 2, 4, 16,$ and 32 \AA because of the calculation cost. The other parameters are fiducial values in Table 1. The solid, dashed, and dotted lines show the averages of the 10 runs, our corrected analytical formula (Equation (11)), and the analytical formula (Equation (9)) of Kataoka et al. (2013b), respectively.

the analytical formula (Equation (9)) of Kataoka et al. (2013b). In contrast, for $\phi \lesssim 0.1$, our results are consistent with the prediction from Equation (9). We note that there are fluctuations of lines when $\phi < 10^{-2}$ because dust aggregates are not attached to all computational boundaries.

4. DISCUSSIONS

In this section, we discuss parameter dependences and the physics behind the compressive strength of dust aggregates. First, we correct the analytical formula of compressive strength with volume filling factors higher than 0.1 in Section 4.1. Second, we discuss the physical validity of the formulated compressive strength in terms of monomer disruption in Section 4.2. Third, we show the energy dissipation mechanisms during the compression in Section 4.3. Finally, we compare our results with previous experimental and numerical studies in Section 4.4 to confirm the validity of our results and discuss interpretations of experimental results.

4.1. Corrected Formula of Compressive Strength

We have shown in Section 3 that the simple formula of Kataoka et al. (2013b) (Equation (9)) underestimates the compressive strength at $\phi > 0.1$. Here, we propose

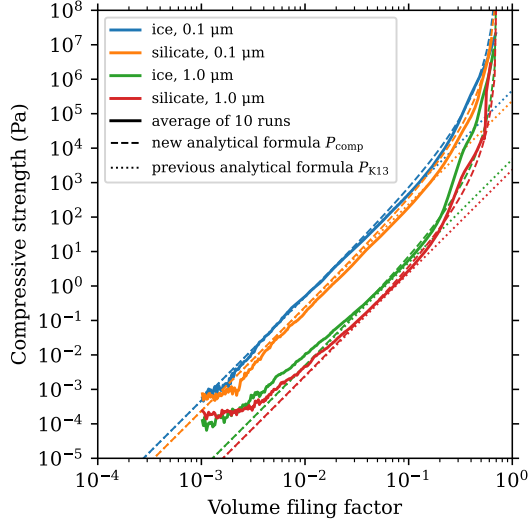


Figure 4. Compressive strength against volume filling factor of dust aggregates with different monomer radii and materials. The colors represent 0.1- μm -radius ice (blue), 1.0- μm -radius ice (green), 0.1- μm -radius silicate (orange), and 1.0- μm -radius silicate (red). The parameters are listed in Table 1. The solid, dashed, and dotted lines show the averages of the 10 runs, our corrected analytical formula (Equation (11)), and the analytical formula (Equation (9)) of Kataoka et al. (2013b), respectively.

a corrected formula applicable to both low and high volume filling factors.

The reason why the previous formula is inaccurate for high volume filling factors is that it neglects the finite volume of monomers. In this regard, the previous formula is similar to the equation of state for ideal gases, in which the pressure neglects the volume occupied by molecules. As is well known, the ideal gas law breaks down at high densities where the inter-molecular volume is small compared to the volume occupied by the molecules. Van der Waals' equation of state for real gases takes the finite volume of the molecules into account by simply subtracting the excluded volume from the volume in the ideal gas law. We expect that a similar correction should improve the accuracy of the previous compressive strength formula.

The correction is as follows. First, we invert Equation (9) as

$$P_{\text{comp}} = \frac{E_{\text{roll}}}{r_0^3} \phi'^3 = \frac{E_{\text{roll}}}{r_0^3} \left(\frac{NV_0}{V'} \right)^3, \quad (10)$$

where $V_0 = (4/3)\pi r_0^3$ is the volume of a monomer. Here, we assume that V' is the volume of the void of dust aggregates, not the volume of dust aggregates. The volume of the void is almost the same as the volume of dust aggregates when $\phi \lesssim 0.1$, while there is a difference be-

tween them when $\phi > 0.1$. Second, we determine the excluded volume that cannot be used for compression. The volume of all monomers NV_0 is the excluded volume. In addition, the void of the closest packed aggregates $V_{\text{cp}} - NV_0$ is the excluded volume, where V_{cp} is the volume of the closest packed aggregates. Therefore, we determine the excluded volume as $NV_0 + V_{\text{cp}} - NV_0 = V_{\text{cp}}$. By using the volume filling factor of the closest packed aggregates $\phi_{\text{max}} = NV_0/V_{\text{cp}}$, we determine the excluded volume as $V_{\text{cp}} = NV_0/\phi_{\text{max}}$. Finally, we obtain the compressive strength of dust aggregates as

$$\begin{aligned} P_{\text{comp}} &= \frac{E_{\text{roll}}}{r_0^3} \left(\frac{NV_0}{V - NV_0/\phi_{\text{max}}} \right)^3 \\ &= \frac{E_{\text{roll}}}{r_0^3} \left(\frac{1}{\phi} - \frac{1}{\phi_{\text{max}}} \right)^{-3} \\ &\simeq 4.7 \times 10^5 \text{ Pa} \left(\frac{\gamma}{100 \text{ mJ m}^{-2}} \right) \left(\frac{r_0}{0.1 \mu\text{m}} \right)^{-2} \\ &\quad \times \left(\frac{\xi_{\text{crit}}}{8 \text{ \AA}} \right) \left(\frac{1}{\phi} - \frac{1}{\phi_{\text{max}}} \right)^{-3}. \end{aligned} \quad (11)$$

Equation (11) shows that the compressive strength diverges at ϕ_{max} .

To compare our simulation results with the corrected analytical formula, we invert Equation (11) into ϕ as a function of P because the input parameter is P and the output parameter is ϕ in the applicative situations, such as experiments. The volume filling factor determined by Equation (11) is given as

$$\phi_{\text{comp}} = \left(\frac{E_{\text{roll}}^{1/3}}{r_0 P^{1/3}} + \frac{1}{\phi_{\text{max}}} \right)^{-1}. \quad (12)$$

We assume $\phi_{\text{max}} = \sqrt{2}\pi/6 = 0.74$, which is the volume filling factor of the hexagonal close-packed and face-centered cubic structures. We also invert Equation (9) as

$$\phi_{\text{K13}} = \frac{r_0 P^{1/3}}{E_{\text{roll}}^{1/3}} \quad (13)$$

to compare the corrected analytical formula with the previous formula.

We confirm that the corrected analytical formula is a much better approximation than the previous formula. In the top panel of Figure 5, we plot the corrected analytical formula for the volume filling factor ϕ_{comp} (Equation (12)), the previous formula ϕ_{K13} (Equation (13)), and the calculated volume filling factors of numerical simulations. We plot them for $P \geq 1$ Pa to focus on when $\phi > 0.1$. We note that monomers in our simulations can deform elastically, so that the volume filling factor could be higher than that of the hexagonal

close-packed and face-centered cubic structures. In the bottom panel of Figure 5, we plot errors between the calculated volume filling factor and the corrected analytical formula and between the calculated volume filling factor and the previous formula, which are given as $|\phi_{\text{calc}} - \phi_{\text{comp}}|$ and $|\phi_{\text{calc}} - \phi_{\text{K13}}|$, respectively. The absolute errors are smaller than 0.1 for most cases of the corrected analytical formula. The error would be due to the complexity of numerical simulations, for example, monomers can deform elastically.

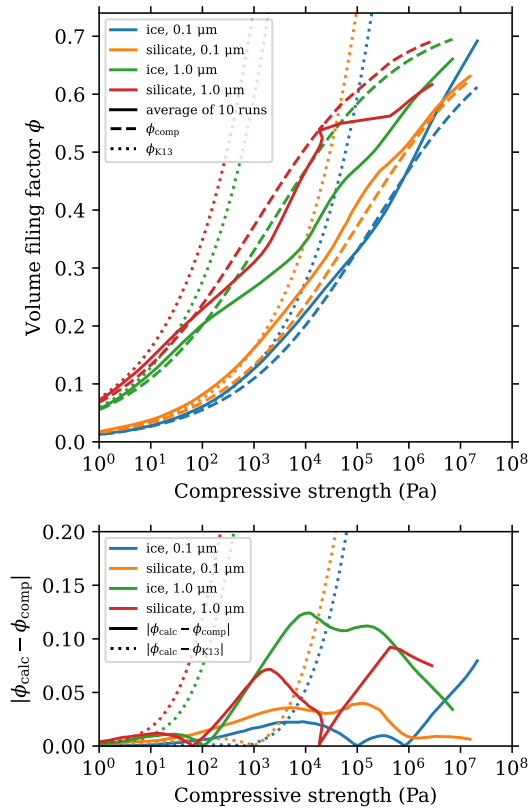


Figure 5. *Top:* volume filling factor against compressive strength of dust aggregates with different monomer radii and materials. The colors show 0.1- μm -radius ice (blue), 1.0- μm -radius ice (green), 0.1- μm -radius silicate (orange), and 1.0- μm -radius silicate (red). The parameters are listed in Table 1. The solid, dashed, and dotted lines show the calculated volume filling factor ϕ_{calc} , the corrected analytical formula ϕ_{comp} (Equation (12)), and the previous formula ϕ_{K13} (Equation (13)), respectively. *Bottom:* absolute error between the calculated volume filling factor and that of the corrected analytical formula (solid) and between the calculated volume filling factor and that of the previous formula (dotted).

4.2. Monomer Disruption

In this section, we discuss the range of the volume filling factor for which compressive strength can be ap-

plied. If the compressive strength is too high, monomers can be broken, and then it could be different from our results.

The strength that materials can be broken has been investigated in the context of material science. For example, ice can be broken at 5–25 MPa when the temperature is from -10°C to -20°C (Haynes 1978; Petrovic 2003). Silica glasses, on the other hand, can be broken at ~ 5 GPa at room temperature (Proctor et al. 1967; Brückner 1970; Kurkjian et al. 2003).

First of all, we note that the stress applied to the contact surface between monomers can be higher than the compressive strength because the stress is concentrated on the area of the contact surface $a^2 \ll r_0^2$, where a is the radius of the contact surface. We assume this stress by assuming the equilibrium radius of the contact surface given by Wada et al. (2007) as

$$\begin{aligned} a_0 &= \left(\frac{9\pi\gamma r_0^2}{4E^*} \right)^{1/3} \\ &\simeq 0.012 \mu\text{m} \left(\frac{\gamma}{100 \text{ mJ m}^{-2}} \right)^{1/3} \\ &\quad \times \left(\frac{r_0}{0.1 \mu\text{m}} \right)^{2/3} \left(\frac{E^*}{3.7 \text{ GPa}} \right)^{-1/3}. \end{aligned} \quad (14)$$

The stress applied to the contact surface is $(a_0/r_0)^2$ times as large as the compressive strength.

By considering both the strength that materials can be broken and the stress applied to the contact surface, we can estimate the upper limit to which the compressive strength formula (Equation (11)) can be applied. We can estimate the upper limit of the compressive strength as

$$\begin{aligned} P_{\text{ul}} &\sim P_{\text{dis}} \left(\frac{a_0}{r_0} \right)^2 \\ &\simeq 0.014 P_{\text{dis}} \left(\frac{\gamma}{100 \text{ mJ m}^{-2}} \right)^{2/3} \\ &\quad \times \left(\frac{r_0}{0.1 \mu\text{m}} \right)^{-2/3} \left(\frac{E^*}{3.7 \text{ GPa}} \right)^{-2/3}, \end{aligned} \quad (15)$$

where P_{dis} is the strength that materials can be disrupted. Here, we assume $P_{\text{dis}} = 10$ MPa and 1 GPa for ice and silicate, respectively. Then, we can also estimate the upper limit of the volume filling factor as

$$\phi_{\text{ul}} = \left(\frac{E_{\text{roll}}^{1/3}}{r_0 P_{\text{ul}}^{1/3}} + \frac{1}{\phi_{\text{max}}} \right)^{-1}. \quad (16)$$

We plot the upper limit of both the compressive strength (Equation (15)) and the volume filling factor (Equation (16)) in Figure 6. The upper limit of the volume filling

factor depends on the monomer radius as well as the material, we find that the upper limits are ~ 0.36 , ~ 0.53 , ~ 0.53 , and ~ 0.64 in the case of ice $0.1 \mu\text{m}$, ice $1.0 \mu\text{m}$, silicate $0.1 \mu\text{m}$, and silicate $1.0 \mu\text{m}$, respectively.

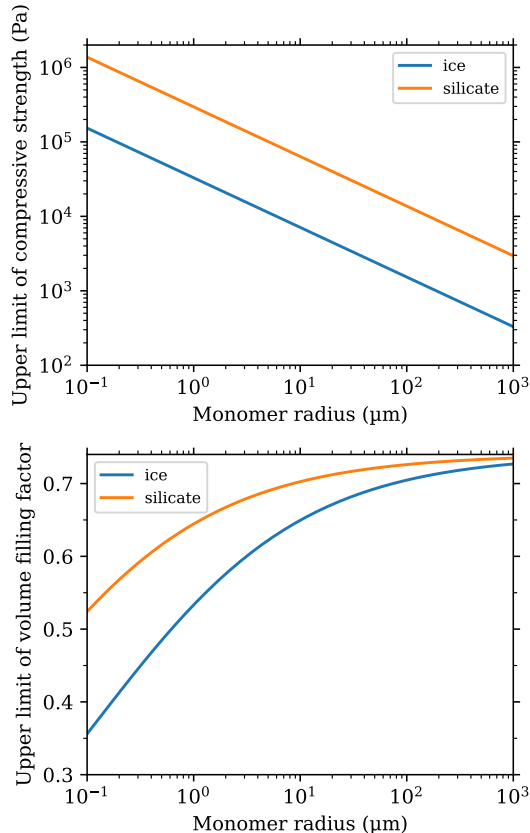


Figure 6. *Top:* upper limit of compressive strength for which monomer disruption can be neglected as a function of monomer radius (Equation (15)). The blue and orange lines are for ice and silicate, respectively. The parameters are listed in Table 1. *Bottom:* upper limit of volume filling factor for which monomer disruption can be neglected as a function of monomer radius (Equation (16)).

4.3. Energy Dissipation Mechanisms

We find that the twisting and sliding motions dominate for high volume filling factors ($\phi > 0.3$), while the dominant energy dissipation mechanism is the rolling motion for low volume filling factors ($10^{-2} < \phi < 0.3$). This is shown in Figure 7, where we plot all energy dissipations of the four cases (ice $0.1 \mu\text{m}$, ice $1.0 \mu\text{m}$, silicate $0.1 \mu\text{m}$, and silicate $1.0 \mu\text{m}$) listed in Table 1. The reason why the twisting and sliding motions dominate for high volume filling factors is as follows. The coordination number defined as the average number of connections per monomer of initial BCCAs is $\simeq 2$. It increases toward $\simeq 3$ for high volume filling factors ($\phi > 0.3$) (see

Figure 3 in Arakawa et al. 2019). For such a large coordination number, monomers are hard to roll and have to twist and slide to increase the volume filling factor.

In some cases, the energy dissipation due to damping motion dominates for very low volume filling factors ($\phi < 10^{-2}$). We cannot obtain the correct compressive strength when damping motion dominates. However, this is not a problem because we focus on the difference between compressive strengths when $\phi \lesssim 0.1$ and $\phi > 0.1$ in this work.

4.4. Comparison with Previous Studies

There are several experimental and numerical studies about the quasi-static compressive strength of spherical silicate and SiO_2 aggregates with volume filling factors higher than 0.1 (e.g., Güttler et al. 2009; Seizinger et al. 2012; Omura & Nakamura 2017, 2018, 2021). Seizinger et al. (2012) performed numerical simulations, in which they prepared a silicate aggregate with a monodisperse monomer size distribution enclosed in a box with fixed boundaries on all sides, and moved the top boundary downwards to mimic the experiments of Güttler et al. (2009). They used the fitting formula of volume filling factor ϕ_{G09} obtained by Güttler et al. (2009) given as

$$\phi_{\text{G09}} = \phi_2 - \frac{\phi_2 - \phi_1}{\exp[(\log_{10} P - \log_{10} p_m)/\Delta] + 1}, \quad (17)$$

where $\phi_1 = 0.15$, $\phi_2 = 0.58$, $p_m = 16.667 \text{ kPa}$, and $\Delta = 0.562$. Recently, Omura & Nakamura (2021) fitted the experimental results of Omura & Nakamura (2017, 2018). They used the same experimental setups as Güttler et al. (2009), but SiO_2 aggregates with a polydisperse size distribution. Omura & Nakamura (2021) used the polytropic relationship given as

$$P = K_p \rho^{(n_p+1)/n_p} = K'_p \phi^{(n_p+1)/n_p}, \quad (18)$$

where K_p and K'_p are constants, ρ is the density, and n_p is the polytropic index. To obtain the volume filling factor as a function of compressive strength, we invert Equation (18) as

$$\phi_{\text{O21}} = \left(\frac{P}{K'_p} \right)^{n_p/(n_p+1)}. \quad (19)$$

Their fitting results are listed in Table 2.

To compare our results with previous ones, we plot them in Figure 8. We use the fitting formulas of experiments: Equation (17) and Equation (19). We compare our results with the previous numerical study (Seizinger et al. 2012), the previous experimental study of SiO_2 aggregates with a monodisperse monomer size distribution (Güttler et al. 2009), and then previous experimental

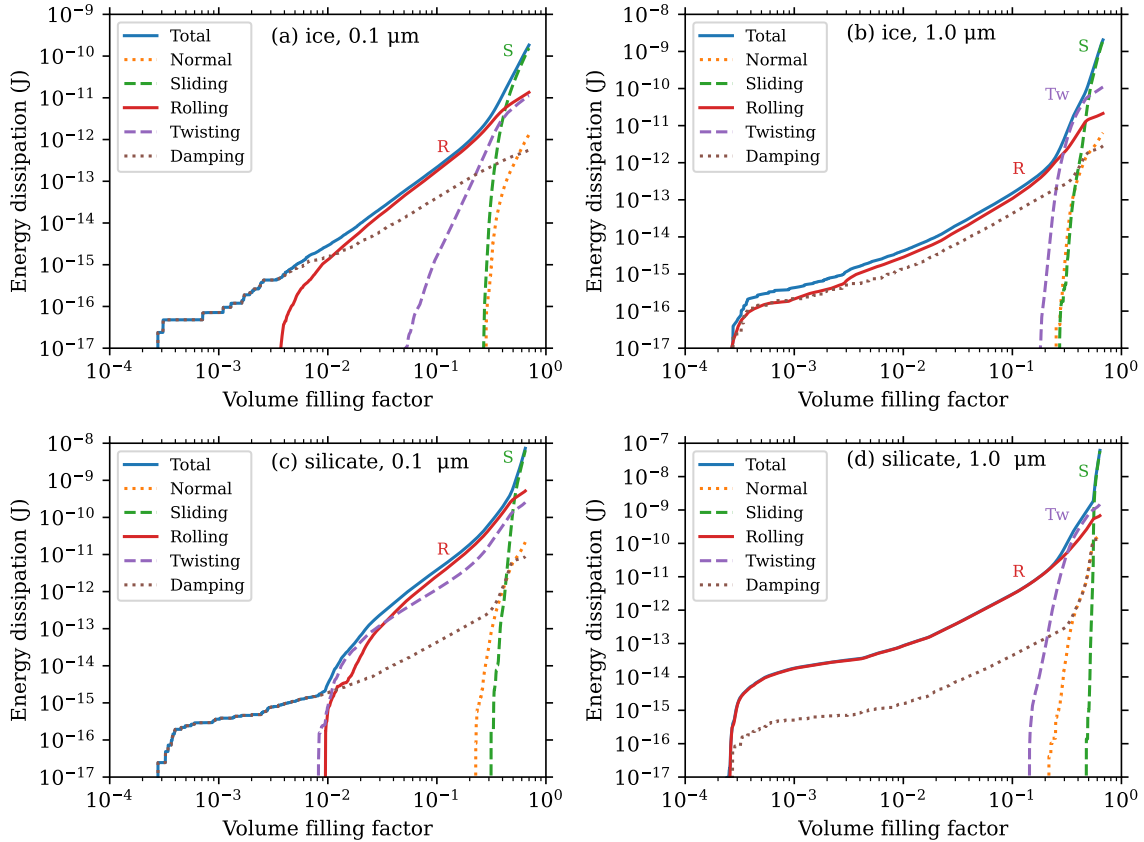


Figure 7. Energy dissipations of (a) 0.1- μm -radius ice, (b) 1.0- μm -radius ice, (c) 0.1- μm -radius silicate, and (d) 1.0- μm -radius silicate. The energy dissipation mechanisms are the normal (orange dotted), sliding (green dashed), rolling (red solid), twisting (purple dashed), damping motions (brown dotted), and the total of all energy dissipations (blue solid). The parameters are listed in Table 1.

studies with a polydisperse size distribution (Omura & Nakamura 2021).

In the left panel of Figure 8, our results are in good agreement with previous numerical results. However, there is a little difference between them because of the different compression setups: to move only the top boundary (Seizinger et al. 2012) or all boundaries (this work). We find that this difference in compression setups is negligible.

In the case of the previous experimental study of SiO_2 aggregates with a monodisperse monomer size distribution (Güttler et al. 2009), the left panel of Figure 8 shows that there is a discrepancy between their results and our analytical formula ϕ_{comp} . This discrepancy may arise from the difference in surface energy. In our simulations, we assume that the surface energy of silicate (SiO_2) is $\gamma = 20 \text{ mJ m}^{-2}$, but some studies suggest that it can be higher (e.g., Yamamoto et al. 2014; Kimura et al. 2015). Therefore, we search for the best-fitted surface energy and find that ϕ_{comp} with $\gamma \simeq 210 \pm 90 \text{ mJ m}^{-2}$ is in good agreement with the experimental results of

Güttler et al. (2009) as shown in the right panel of Figure 8.

We also explain the previous experimental results of SiO_2 aggregates with a polydisperse monomer size distribution (Omura & Nakamura 2021) by assuming a higher surface energy than $\gamma = 20 \text{ mJ m}^{-2}$. The left panel of Figure 8 shows that there is a discrepancy between their results and our analytical formula ϕ_{comp} when $\gamma = 20 \text{ mJ m}^{-2}$, while the right panel shows that their results are in good agreement with ϕ_{comp} when $\gamma = 210 \text{ mJ m}^{-2}$. However, there remains a discrepancy, especially for a larger monomer radius. When the monomer size distribution is polydisperse, larger monomers get stuck at first during aggregate compression, and then smaller monomers get stuck. We interpret this discrepancy as the uncertainty of the volume filling factor of realistic dust aggregates which have a monomer size distribution.

5. CONCLUSIONS

Table 2. Fitting results of compression experiments of Omura & Nakamura (2021)

Name	Median radius (μm)	K'_p (Pa)	n_p	Fitting range	
				Min (Pa)	Max (Pa)
Silica beads	0.85	$(8.35 \pm 0.23) \times 10^6$	$(2.201 \pm 0.013) \times 10^{-1}$	3.2×10^3	4.0×10^5
Fly ash	2.4	$(1.649 \pm 0.025) \times 10^8$	$(8.134 \pm 0.014) \times 10^{-2}$	1.0×10^3	3.9×10^5
Glass beads	9	$(2.951 \pm 0.093) \times 10^{16}$	$(2.3496 \pm 0.0027) \times 10^{-2}$	1.0×10^3	3.9×10^5

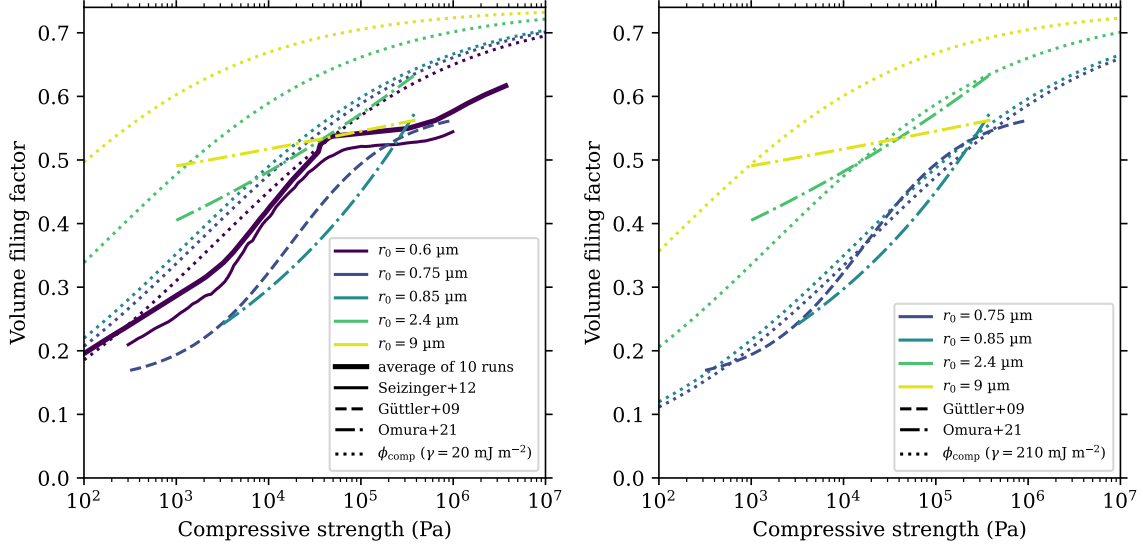


Figure 8. *Left:* volume filling factor against compressive strength of this work and previous studies. The monomer radii are $r_0 = 0.6, 0.75, 0.85, 2.4,$ and $9 \mu\text{m}$ from dark to light colors in all line types. The thick and thin solid lines show the numerical results of silicate aggregates of this work and Seizinger et al. (2012), respectively. The other parameters of silicate are listed in Table 1, but we adopt that $C_v = 3 \times 10^{-7}$. The dashed and dash-dotted lines show the experimental results of SiO_2 aggregates with a monodisperse (Güttler et al. 2009) and polydisperse monomer size distribution (Omura & Nakamura 2021), respectively. We use Equation (17) and Equation (19) as the fitting results of Güttler et al. (2009) and Omura & Nakamura (2021), respectively. We also use the values listed in Table 2. The dotted lines show the analytical formula ϕ_{comp} (Equation (12)) of silicate aggregates. *Right:* the dotted lines are the same as those of the left panel, but we change the surface energy to be $\gamma = 210 \text{ mJ m}^{-2}$.

We performed numerical simulations of the compression of dust aggregates and formulated the compressive strength that can treat a full range of volume filling factors. We used a monomer interaction model based on Dominik & Tielens (1997) and Wada et al. (2007). In our simulations, we created a BCCA at first and compressed it sufficiently slowly and three-dimensionally by moving periodic boundaries. We calculated the compressive strength by using the translational kinetic energy and the sum of the forces acting at all connections per unit volume. For every parameter set, we performed 10 simulations with different initial BCCAs and took an average of them.

Our main findings of the compressive strength of dust aggregates are as follows.

1. As a result of numerical simulations, we found that the compressive strength becomes sharply harder when the volume filling factor exceeds 0.1. We also found that the compressive strength for high volume filling factors ($\phi \gtrsim 0.3$) does not depend on the critical rolling displacement.
2. We corrected the analytical formula of compressive strength by taking into account the closest packing of aggregates for high volume filling factors. The corrected formula is given by Equation (11) in Section 4.1 as follows:

$$P_{\text{comp}} = \frac{E_{\text{roll}}}{r_0^3} \left(\frac{1}{\phi} - \frac{1}{\phi_{\text{max}}} \right)^{-3}$$

$$\simeq 4.7 \times 10^5 \text{ Pa} \left(\frac{\gamma}{100 \text{ mJ m}^{-2}} \right) \left(\frac{r_0}{0.1 \mu\text{m}} \right)^{-2} \times \left(\frac{\xi_{\text{crit}}}{8 \text{ \AA}} \right) \left(\frac{1}{\phi} - \frac{1}{\phi_{\text{max}}} \right)^{-3}, \quad (20)$$

where E_{roll} is the energy needed for a monomer to roll a distance of $(\pi/2)r_0$ (Equation (1)), r_0 is the monomer radius, $\phi_{\text{max}} = \sqrt{2}\pi/6 = 0.74$ is the volume filling factor of the closest packing, γ is the surface energy, and ξ_{crit} is the critical rolling displacement. We confirmed that the corrected analytical formula reproduces our simulation results including parameter dependences. In terms of the monomer disruption, the corrected formula is valid for $\phi \lesssim 0.36, 0.53, 0.53,$ and 0.64 in the case of $0.1\text{-}\mu\text{m}$ -radius ice, $1.0\text{-}\mu\text{m}$ -radius ice, $0.1\text{-}\mu\text{m}$ -radius silicate, and $0.1\text{-}\mu\text{m}$ -radius silicate monomers, respectively.

3. We found that twisting and sliding motions dominate for high volume filling factors ($\phi > 0.3$), while rolling motion dominates for low volume filling fac-

tors ($\phi < 0.3$). We explained the reason why the twisting and sliding motions dominate by the increase of coordination number.

4. Our numerical results are consistent with the previous numerical results (Seizinger et al. 2012). However, there is a discrepancy between the previous experimental results (Güttler et al. 2009) and our analytical formula. We found that our analytical formula is consistent with the experimental results if we assume the surface energy of silicate is $\simeq 210 \pm 90 \text{ mJ m}^{-2}$.

This work was supported by JSPS KAKENHI Grant Numbers JP19J20351 and JP22J00260. This work has made use of NASA's Astrophysics Data System. This work has made use of adstex (<https://github.com/yymao/adstex>).

Software: VisIt (Childs et al. 2012)

REFERENCES

- Arakawa, S., Tatsuuma, M., Sakatani, N., & Nakamoto, T. 2019, *Icarus*, 324, 8, doi: [10.1016/j.icarus.2019.01.022](https://doi.org/10.1016/j.icarus.2019.01.022)
- Blum, J., & Schräpler, R. 2004, *PhRvL*, 93, 115503, doi: [10.1103/PhysRevLett.93.115503](https://doi.org/10.1103/PhysRevLett.93.115503)
- Blum, J., & Wurm, G. 2000, *Icarus*, 143, 138, doi: [10.1006/icar.1999.6234](https://doi.org/10.1006/icar.1999.6234)
- Brückner, R. 1970, *Journal of Non-Crystalline Solids*, 5, 123, doi: [https://doi.org/10.1016/0022-3093\(70\)90190-0](https://doi.org/10.1016/0022-3093(70)90190-0)
- Childs, H., Brugger, E., Whitlock, B., et al. 2012, *VisIt: An End-User Tool For Visualizing and Analyzing Very Large Data*, doi: [10.1201/b12985](https://doi.org/10.1201/b12985)
- Davidsson, B. J. R., Sierks, H., Güttler, C., et al. 2016, *A&A*, 592, A63, doi: [10.1051/0004-6361/201526968](https://doi.org/10.1051/0004-6361/201526968)
- Dominik, C., & Tielens, A. G. G. M. 1997, *ApJ*, 480, 647, doi: [10.1086/303996](https://doi.org/10.1086/303996)
- Fulle, M., Blum, J., Green, S. F., et al. 2019, *MNRAS*, 482, 3326, doi: [10.1093/mnras/sty2926](https://doi.org/10.1093/mnras/sty2926)
- Geretshauser, R. J., Meru, F., Speith, R., & Kley, W. 2011, *A&A*, 531, A166, doi: [10.1051/0004-6361/201116901](https://doi.org/10.1051/0004-6361/201116901)
- Geretshauser, R. J., Speith, R., Güttler, C., Krause, M., & Blum, J. 2010, *A&A*, 513, A58, doi: [10.1051/0004-6361/200913596](https://doi.org/10.1051/0004-6361/200913596)
- Greenwood, J. A., & Johnson, K. L. 2006, *Journal of Colloid and Interface Science*, 296, 284, doi: [10.1016/j.jcis.2005.08.069](https://doi.org/10.1016/j.jcis.2005.08.069)
- Güttler, C., Krause, M., Geretshauser, R. J., Speith, R., & Blum, J. 2009, *ApJ*, 701, 130, doi: [10.1088/0004-637X/701/1/130](https://doi.org/10.1088/0004-637X/701/1/130)
- Haynes, F. D. 1978, *Effect of temperature on the strength of snow-ice*, Department of the Army, Cold Regions Research and Engineering Laboratory, Corps of Engineers, CRRELReport 78-27, Hanover, New Hampshire
- Heim, L.-O., Blum, J., Preuss, M., & Butt, H.-J. 1999, *PhRvL*, 83, 3328, doi: [10.1103/PhysRevLett.83.3328](https://doi.org/10.1103/PhysRevLett.83.3328)
- Israelachvili, J. N. 1992, *Surface Science Reports*, 14, 109, doi: [10.1016/0167-5729\(92\)90015-4](https://doi.org/10.1016/0167-5729(92)90015-4)
- Johansen, A., Oishi, J. S., Mac Low, M.-M., et al. 2007, *Nature*, 448, 1022, doi: [10.1038/nature06086](https://doi.org/10.1038/nature06086)
- Johnson, K. L., Kendall, K., & Roberts, A. D. 1971, *Proceedings of the Royal Society of London Series A*, 324, 301, doi: [10.1098/rspa.1971.0141](https://doi.org/10.1098/rspa.1971.0141)
- Kataoka, A., Tanaka, H., Okuzumi, S., & Wada, K. 2013a, *A&A*, 557, L4, doi: [10.1051/0004-6361/201322151](https://doi.org/10.1051/0004-6361/201322151)
- . 2013b, *A&A*, 554, A4, doi: [10.1051/0004-6361/201321325](https://doi.org/10.1051/0004-6361/201321325)
- Kempf, S., Pfalzner, S., & Henning, T. K. 1999, *Icarus*, 141, 388, doi: [10.1006/icar.1999.6171](https://doi.org/10.1006/icar.1999.6171)
- Kimura, H., Wada, K., Senshu, H., & Kobayashi, H. 2015, *ApJ*, 812, 67, doi: [10.1088/0004-637X/812/1/67](https://doi.org/10.1088/0004-637X/812/1/67)

- Krause, M., & Blum, J. 2004, *PhRvL*, 93, 021103, doi: [10.1103/PhysRevLett.93.021103](https://doi.org/10.1103/PhysRevLett.93.021103)
- Krijt, S., Güttler, C., Heißelmann, D., Dominik, C., & Tielens, A. G. G. M. 2013, *Journal of Physics D Applied Physics*, 46, 435303, doi: [10.1088/0022-3727/46/43/435303](https://doi.org/10.1088/0022-3727/46/43/435303)
- Krijt, S., Schwarz, K. R., Bergin, E. A., & Ciesla, F. J. 2018, *ApJ*, 864, 78, doi: [10.3847/1538-4357/aad69b](https://doi.org/10.3847/1538-4357/aad69b)
- Kurkjian, C., Gupta, P., Brow, R., & Lower, N. 2003, *Journal of Non-Crystalline Solids*, 316, 114, doi: [https://doi.org/10.1016/S0022-3093\(02\)01943-9](https://doi.org/10.1016/S0022-3093(02)01943-9)
- Lorek, S., Lacerda, P., & Blum, J. 2018, *A&A*, 611, A18, doi: [10.1051/0004-6361/201630175](https://doi.org/10.1051/0004-6361/201630175)
- Meakin, P. 1991, *Reviews of Geophysics*, 29, 317, doi: [10.1029/91RG00688](https://doi.org/10.1029/91RG00688)
- Mukai, T., Ishimoto, H., Kozasa, T., Blum, J., & Greenberg, J. M. 1992, *A&A*, 262, 315
- Okuzumi, S., Tanaka, H., Kobayashi, H., & Wada, K. 2012, *ApJ*, 752, 106, doi: [10.1088/0004-637X/752/2/106](https://doi.org/10.1088/0004-637X/752/2/106)
- Okuzumi, S., Tanaka, H., & Sakagami, M.-a. 2009, *ApJ*, 707, 1247, doi: [10.1088/0004-637X/707/2/1247](https://doi.org/10.1088/0004-637X/707/2/1247)
- Omura, T., & Nakamura, A. M. 2017, *Planet. Space Sci.*, 149, 14, doi: [10.1016/j.pss.2017.08.003](https://doi.org/10.1016/j.pss.2017.08.003)
- . 2018, *ApJ*, 860, 123, doi: [10.3847/1538-4357/aabe81](https://doi.org/10.3847/1538-4357/aabe81)
- . 2021, *PSJ*, 2, 41, doi: [10.3847/PSJ/abdf63](https://doi.org/10.3847/PSJ/abdf63)
- Ossenkopf, V. 1993, *A&A*, 280, 617
- Paszun, D., & Dominik, C. 2006, *Icarus*, 182, 274, doi: [10.1016/j.icarus.2005.12.018](https://doi.org/10.1016/j.icarus.2005.12.018)
- . 2008, *A&A*, 484, 859, doi: [10.1051/0004-6361:20079262](https://doi.org/10.1051/0004-6361:20079262)
- . 2009, *A&A*, 507, 1023, doi: [10.1051/0004-6361/200810682](https://doi.org/10.1051/0004-6361/200810682)
- Petrovic, J. J. 2003, *Journal of Materials Science*, 38, 1, doi: [10.1023/A:1021134128038](https://doi.org/10.1023/A:1021134128038)
- Proctor, B. A., Whitney, I., Johnson, J. W., & Cottrell, A. H. 1967, *Proceedings of the Royal Society of London. Series A. Mathematical and Physical Sciences*, 297, 534, doi: [10.1098/rspa.1967.0085](https://doi.org/10.1098/rspa.1967.0085)
- Seizinger, A., Speith, R., & Kley, W. 2012, *A&A*, 541, A59, doi: [10.1051/0004-6361/201218855](https://doi.org/10.1051/0004-6361/201218855)
- Smirnov, B. M. 1990, *PhR*, 188, 1, doi: [10.1016/0370-1573\(90\)90010-Y](https://doi.org/10.1016/0370-1573(90)90010-Y)
- Suyama, T., Wada, K., & Tanaka, H. 2008, *ApJ*, 684, 1310, doi: [10.1086/590143](https://doi.org/10.1086/590143)
- Suyama, T., Wada, K., Tanaka, H., & Okuzumi, S. 2012, *ApJ*, 753, 115, doi: [10.1088/0004-637X/753/2/115](https://doi.org/10.1088/0004-637X/753/2/115)
- Tanaka, H., Wada, K., Suyama, T., & Okuzumi, S. 2012, *Progress of Theoretical Physics Supplement*, 195, 101, doi: [10.1143/PTPS.195.101](https://doi.org/10.1143/PTPS.195.101)
- Tatsuuma, M., Kataoka, A., & Tanaka, H. 2019, *ApJ*, 874, 159, doi: [10.3847/1538-4357/ab09f7](https://doi.org/10.3847/1538-4357/ab09f7)
- Wada, K., Tanaka, H., Okuzumi, S., et al. 2013, *A&A*, 559, A62, doi: [10.1051/0004-6361/201322259](https://doi.org/10.1051/0004-6361/201322259)
- Wada, K., Tanaka, H., Suyama, T., Kimura, H., & Yamamoto, T. 2007, *ApJ*, 661, 320, doi: [10.1086/514332](https://doi.org/10.1086/514332)
- . 2008, *ApJ*, 677, 1296, doi: [10.1086/529511](https://doi.org/10.1086/529511)
- . 2009, *ApJ*, 702, 1490, doi: [10.1088/0004-637X/702/2/1490](https://doi.org/10.1088/0004-637X/702/2/1490)
- . 2011, *ApJ*, 737, 36, doi: [10.1088/0004-637X/737/1/36](https://doi.org/10.1088/0004-637X/737/1/36)
- Wahlberg Jansson, K., Johansen, A., Bukhari Syed, M., & Blum, J. 2017, *ApJ*, 835, 109, doi: [10.3847/1538-4357/835/1/109](https://doi.org/10.3847/1538-4357/835/1/109)
- Windmark, F., Birnstiel, T., Ormel, C. W., & Dullemond, C. P. 2012, *A&A*, 544, L16, doi: [10.1051/0004-6361/201220004](https://doi.org/10.1051/0004-6361/201220004)
- Wurm, G., & Blum, J. 1998, *Icarus*, 132, 125, doi: [10.1006/icar.1998.5891](https://doi.org/10.1006/icar.1998.5891)
- Yamamoto, T., Kadono, T., & Wada, K. 2014, *ApJL*, 783, L36, doi: [10.1088/2041-8205/783/2/L36](https://doi.org/10.1088/2041-8205/783/2/L36)
- Yang, C.-C., Johansen, A., & Carrera, D. 2017, *A&A*, 606, A80, doi: [10.1051/0004-6361/201630106](https://doi.org/10.1051/0004-6361/201630106)

APPENDIX

A. DERIVATION OF COMPRESSIVE STRENGTH

In this appendix, we explain the detailed derivation of compressive strength related to Section 2.3.

The equation of motion of monomer i is given as

$$m_0 \frac{d^2 \mathbf{x}_i}{dt^2} = \mathbf{W}_i + \mathbf{F}_i, \quad (\text{A1})$$

where \mathbf{W}_i is the force exerted from the computational boundaries on monomer i and \mathbf{F}_i is the total force from other monomers on monomer i . The compressive strength relates to \mathbf{W}_i .

To describe the first term on the right-hand side of Equation (A1) by using the compressive strength, we take an inner product of \mathbf{x}_i and Equation (A1), and take a long-time average with time interval τ . The left-hand side of Equation (A1) becomes

$$\frac{m_0}{\tau} \int_0^\tau \mathbf{x}_i \cdot \frac{d^2 \mathbf{x}_i}{dt^2} dt = \frac{m_0}{\tau} \left[\mathbf{x}_i \cdot \frac{d\mathbf{x}_i}{dt} \right]_0^\tau - \frac{m_0}{\tau} \int_0^\tau \frac{d\mathbf{x}_i}{dt} \cdot \frac{d\mathbf{x}_i}{dt} dt. \quad (\text{A2})$$

The first term on the right-hand side of Equation (A2) vanishes when $\tau \rightarrow \infty$. Writing a long-time average as $\langle \rangle_t$ and summing Equation (A1) over all i , we have

$$\left\langle \sum_{i=1}^N \frac{m_0}{2} \left(\frac{d\mathbf{x}_i}{dt} \right)^2 \right\rangle_t = -\frac{1}{2} \left\langle \sum_{i=1}^N \mathbf{x}_i \cdot \mathbf{W}_i \right\rangle_t - \frac{1}{2} \left\langle \sum_{i=1}^N \mathbf{x}_i \cdot \mathbf{F}_i \right\rangle_t \quad (\text{A3})$$

The left-hand side of Equation (A3) is the time-averaged kinematic energy of all monomers defined as

$$K = \left\langle \sum_{i=1}^N \frac{m_0}{2} \left(\frac{d\mathbf{x}_i}{dt} \right)^2 \right\rangle_t. \quad (\text{A4})$$

The first term on the right-hand side of Equation (A3) relates to the compressive strength P_{calc} . The force on the computational boundary of the area dS_b is $P_{\text{calc}} \mathbf{n}_b dS_b$, where \mathbf{n}_b is the normal vector of the boundary directed outward. Then,

$$\begin{aligned} \left\langle \sum_{i=1}^N \mathbf{x}_i \cdot \mathbf{W}_i \right\rangle_t &= - \int_{S_b} P_{\text{calc}} \mathbf{n}_b \cdot \mathbf{x} dS_b \\ &= -P_{\text{calc}} \int_V \text{div} \mathbf{x} dV \\ &= -P_{\text{calc}} \int_V \left(\frac{\partial x}{\partial x} + \frac{\partial y}{\partial y} + \frac{\partial z}{\partial z} \right) dV \\ &= -3P_{\text{calc}} V. \end{aligned} \quad (\text{A5})$$

The total force from other monomers to monomer i can be described as

$$\mathbf{F}_i = \sum_{j \neq i} \mathbf{f}_{i,j}. \quad (\text{A6})$$

Equations (A3)–(A6) yield

$$P_{\text{calc}} = \frac{2K}{3V} + \frac{1}{3V} \left\langle \sum_{i < j} (\mathbf{x}_i - \mathbf{x}_j) \cdot \mathbf{f}_{i,j} \right\rangle_t \quad (\text{A7})$$

because of the relation that $\mathbf{f}_{i,j} = -\mathbf{f}_{j,i}$.

B. OTHER PARAMETER DEPENDENCES

In this appendix, we show dependences on the number of monomers N , the strain rate parameter C_v , the damping coefficient k_n , and the time-step.

First, we confirm that there is no dependence on the number of monomers, i.e., the size of the calculation box. This is shown in Figure 9, where we plot compressive strength when $N = 1024, 4096, 16384$, and 65536 .

Second, we verify that the strain rate parameter, which refers to the velocity at the computational boundaries, does not exhibit any dependence. This is shown in Figure 10, where we plot compressive strength when $C_v = 1 \times 10^{-7}, 3 \times 10^{-7}$, and 1×10^{-6} . There are fluctuations of compressive strength when $\phi \lesssim 3 \times 10^{-3}$ because dust aggregates are not attached to all computational boundaries. We note that compressive strength in this work is quasi-static, so it does not depend on the velocity at the computational boundaries if it is small enough.

Third, we confirm that the damping coefficient does not exhibit any dependence. This is shown in Figure 11, where we plot compressive strength when $k_n = 0, 0.01$, and 0.1 .

Finally, we verify that the results are not affected by the length of the time-step because the compressive strength in this work is quasi-static. This is shown in Figure 12, where we plot compressive strength in the two cases (ice $0.1 \mu\text{m}$ and ice $1.0 \mu\text{m}$) listed in Table 1 and when the time-step is two times longer.

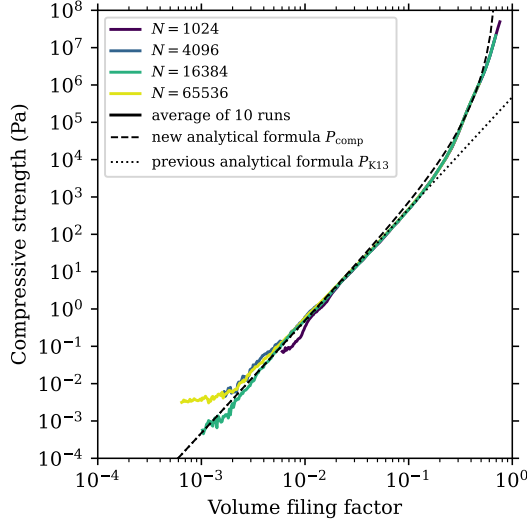


Figure 9. Compressive strength against volume filling factor of dust aggregates that contain ice monomers of $0.1\text{-}\mu\text{m}$ radius with different numbers of monomers N . The numbers of monomers are $N = 1024, 4096, 16384,$ and 65536 from dark to light colors. We adopt $C_v = 3 \times 10^{-7}$ for $N = 1024, 4096,$ and 65536 because of the calculation cost. The other parameters are fiducial values in Table 1. The solid, dashed, and dotted lines show the averages of the 10 runs, our corrected analytical formula (Equation (11)), and the analytical formula (Equation (9)) of Kataoka et al. (2013b), respectively.

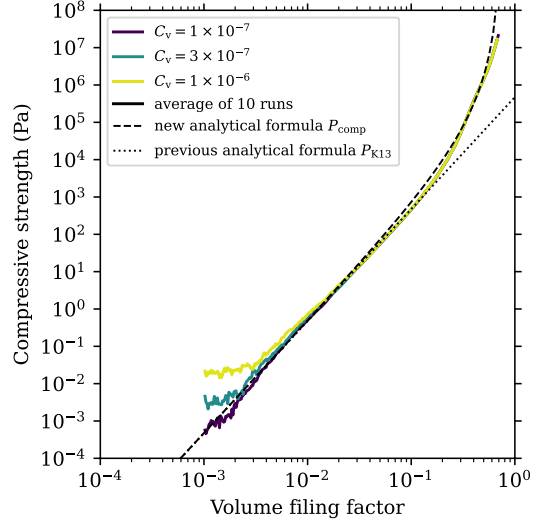


Figure 10. Compressive strength against volume filling factor of dust aggregates that contain ice monomers of $0.1\text{-}\mu\text{m}$ radius with different strain rate parameters C_v . The strain rate parameters are $C_v = 1 \times 10^{-7}, 3 \times 10^{-7},$ and 1×10^{-6} from dark to light colors. The other parameters are fiducial values in Table 1. The solid, dashed, and dotted lines show the averages of the 10 runs, our corrected analytical formula (Equation (11)), and the analytical formula (Equation (9)) of Kataoka et al. (2013b), respectively.

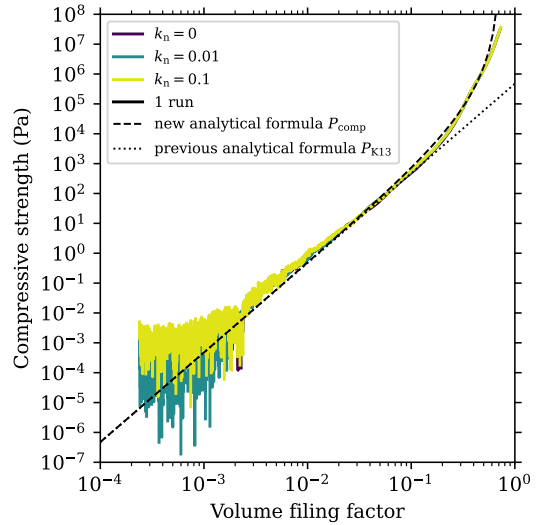


Figure 11. Compressive strength against volume filling factor of dust aggregates that contain ice monomers of $0.1\text{-}\mu\text{m}$ radius with different damping coefficients k_n . The damping coefficients are $k_n = 0, 0.01,$ and 0.1 from dark to light colors. We adopt $C_v = 3 \times 10^{-7}$ for $k_n = 0$ and 0.1 because of the calculation cost. The other parameters are fiducial values in Table 1. The solid, dashed, and dotted lines show the result of a run, our corrected analytical formula (Equation (11)), and the analytical formula (Equation (9)) of Kataoka et al. (2013b), respectively.

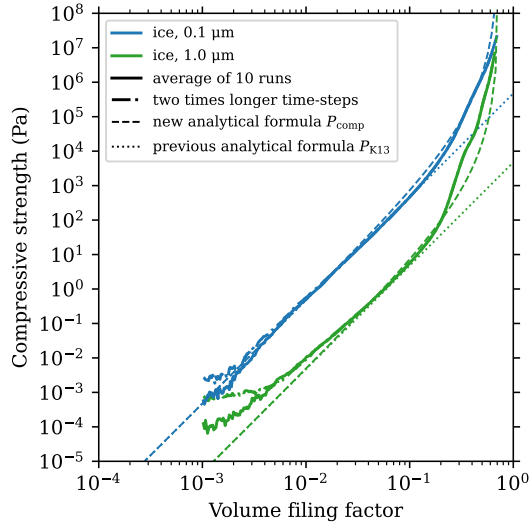


Figure 12. Compressive strength against volume filling factor of dust aggregates that contain ice monomers of $0.1\text{-}\mu\text{m}$ (blue) and $1.0\text{-}\mu\text{m}$ (green) radius with different time-steps. The other parameters are fiducial values in Table 1. The solid, dash-dotted, dashed, and dotted lines show the averages of the 10 runs, the averages of the 10 runs with two times longer time-steps, our corrected analytical formula (Equation (11)), and the analytical formula (Equation (9)) of Kataoka et al. (2013b), respectively. We adopt $C_v = 3 \times 10^{-7}$ for two times longer time-steps because of the calculation cost.